Please cite this article in press as: Prasanna et al., Spatial heterogeneity in tumor adhesion qualifies collective cell invasion, Biophysical Journal (2024), https://doi.org/10.1016/j.bpj.2024.05.005

Biophysical Journal
Article

Biophysical Society

Spatial heterogeneity in tumor adhesion qualifies collective cell invasion

C. Venkata Sai Prasanna,[1] Mohit Kumar Jolly,[2,*] and Ramray Bhat[2,3,*]
[1]IISc Mathematics Initiative, Indian Institute of Science, Bangalore, India; [2]Department of Bioengineering, Indian Institute of Science, Bangalore, India; and [3]Department of Developmental Biology and Genetics, Indian Institute of Science, Bangalore, India

ABSTRACT Collective cell invasion (CCI), a canon of most invasive solid tumors, is an emergent property of the interactions between cancer cells and their surrounding extracellular matrix (ECM). However, tumor populations invariably consist of cells expressing variable levels of adhesive proteins that mediate such interactions, disallowing an intuitive understanding of how tumor invasiveness at a multicellular scale is influenced by spatial heterogeneity of cell-cell and cell-ECM adhesion. Here, we have used a Cellular Potts model-based multiscale computational framework that is constructed on the histopathological principles of glandular cancers. In earlier efforts on homogenous cancer cell populations, this framework revealed the relative ranges of interactions, including cell-cell and cell-ECM adhesion that drove collective, dispersed, and mixed multimodal invasion. Here, we constitute a tumor core of two separate cell subsets showing distinct intra- and inter-subset cell-cell or cell-ECM adhesion strengths. These two subsets of cells are arranged to varying extents of spatial intermingling, which we call the heterogeneity index (HI). We observe that low and high inter-subset cell adhesion favors invasion of high-HI and low-HI intermingled populations with distinct intra-subset cell-cell adhesion strengths, respectively. In addition, for explored values of cell-ECM adhesion strengths, populations with high HI values collectively invade better than those with lower HI values. We then asked how spatial invasion is regulated by progressively intermingled cellular subsets that are epithelial, i.e., showed high cell-cell but poor cell-ECM adhesion, and mesenchymal, i.e., with reversed adhesion strengths to the former. Here too, inter-subset adhesion plays an important role in contextualizing the proportionate relationship between HI and invasion. An exception to this relationship is seen for cases of heterogeneous cell-ECM adhesion where sub-maximal HI patterns with higher outer localization of cells with stronger ECM adhesion collectively invade better than their relatively higher-HI counterparts. Our simulations also reveal how adhesion heterogeneity qualifies collective invasion, when either cell-cell or cell-ECM adhesion type is varied but results in an invasive dispersion when both adhesion types are simultaneously altered.

SIGNIFICANCE In this paper, we sought to investigate the effect of spatial arrangements of tumor cell niches with distinct levels of inter-cell or cell-extracellular matrix adhesion on the overall invasion of the heterogeneous tumor population. For differences in intra-subset cell adhesion, more intermingled niches showed highest invasion when inter-subset cell adhesion was low, and less intermingled niches showed highest invasion when inter-subset cell adhesion was high. For niches with distinct cell-extracellular matrix adhesion, invasion was highest when cells belonging to niche with higher adhesion were localized to the periphery of the tumor population in contact with the extracellular matrix.

INTRODUCTION

Transformed cells from epithelial tissues and organs invade from their locus of origin into their surrounding extracellular matrix (ECM) microenvironment in various ways: groups of cells may move together, a process known as collective cell invasion (CCI); in contrast, single cells can separate out and invade independently of each other, which is called dispersed cell invasion (DCI) (1–3). CCI is a complex process that involves coordination by cells across their moving mass, along with cooperative signaling that allows cells to synchronize their actions across the multicellular spatial scale (4,5). Although adhesion between moving cancer cells, mediated through cadherin-rich adhesion junctions has been proposed to contribute to collective invasion, recent experimental and computational studies suggest this to not be an imperative criterion: non-adherent cancer cell masses may still invade together, albeit in an uncoordinated manner when allowed to move through a confining ECM space (3,6). Interactions with the latter involve both

Submitted October 27, 2023, and accepted for publication May 3, 2024.

*Correspondence: mkjolly@iisc.ac.in or ramray@iisc.ac.in

Editor: Pablo A. Iglesias.

https://doi.org/10.1016/j.bpj.2024.05.005

Please cite this article in press as: Prasanna et al., Spatial heterogeneity in tumor adhesion qualifies collective cell invasion, Biophysical Journal (2024), https://doi.org/10.1016/j.bpj.2024.05.005

adhesion to ECM proteins and proteolytic or non-proteolytic mechanical effects exerted on them by invading cancer cells (7). Thus, CCI is likely influenced by heterogeneous subpopulations of cells with varying adhesive strengths among themselves as well as to the ECM.

Experimental invasion studies performed with cancer cell lines or primary cells isolated from patient tumors frequently presume the interactions between cells or with their surrounding ECM to be similar across the collective mass. Although cytological variegation within tumors has long been reported by pathologists, emerging studies on tumor samples establish heterogeneity at multiple levels including at the scale of proteins mediating inter-cellular or cell-ECM adhesion. Alexander et al. show, for instance, that invasive lobular carcinomas thought to be depleted of E-cadherin may instead show cell-variable heterogeneity in its expression (8). Epigenetic downregulation of E-cadherin driven by the microenvironment may also result in a variegated expression of the protein in ductal breast cancers (9). Heterogeneity has also been observed experimentally for receptors such as integrins, which mediate adhesion with ECM (10,11). Such variation in spatial expression of adhesive proteins suggests concurrent heterogeneity in the force of cell-cell and cell-ECM adhesion and can be associated with patient survival as well (12).

Heterogeneity in molecular expression within tumors can have marked effects on cellular and multicellular phenotypes. One example is patchy mechanical behavior within cell populations, which is confirmed through their rigorous spatial exploration using atomic force microscopy (13). The effects of such heterogeneity on cancer cell invasion are beginning to be elucidated (14–17). Such patchy behaviors can be quantified via persistence length, as quantified through approaches such as topological data analysis of dynamics of collective invasion (18). Although the consequences of variation in the arrangement of adhesive forces across mesoscopic cell scales have been elegantly demonstrated in developmental systems (19–21), such outcomes remain ill-explored in tumor progression. One notable effort by Reher et al. uses a cellular automaton approach to show that the dissemination of cells can be mediated through an increase in spatial heterogeneity in cell adhesion and a loss of control on their adhesion receptor concentrations through the local cellular microenvironment (22). In this paper, we implement a Cellular Potts model (CPM)-based computational multiscale framework that explores the behavior of a population of cells that are encased within an ECM architecture that is mimetic of the histopathological features of glandular tissues in a precancerous stage. We show how the nature of spatial arrangement in cell-cell or cell-ECM-adhesive strengths can have significant effects on the dissemination of such tumor populations. Our results are consistent with, and rationalize, the multiple molecular variations associated with epithelial to mesenchymal transition (EMT) seen in cancers and have implications for the use of biopsies in the diagnosis of invasive cancers.

MATERIALS AND METHODS

Modeling framework and CompuCell3D

CompuCell3D (CC3D) is an agent-based simulation framework that is developed to computationally model systems of cell-, developmental-, and cancer biology. It is primarily based on the CPM/Glazier-Graner-Hogeweg (GGH) model (50). CC3D combines CPM/GGH with partial differential equation solvers for chemical fields and other models for spatio-temporal modeling by defining spatially extended generalized cells, which can represent single biological cells, their clusters, or even subcompartments and subdomains of noncellular materials (51).

The CPM effective energy, the cornerstone of all CC3D simulations describes cell behaviors and interactions by incorporating contact energy terms, which determine the extent of interaction between different cell types in the simulations. Positive contact energy values indicate the extent of repulsion between different entities in the simulation. In the context of biology, it is the adhesion between the entities which has significance and implications. The relation between adhesion and contact energy in CC3D is inverse, i.e., adhesion is negative of contact energy.

$$H = \sum_{i,j} J(\tau(\sigma(i)), \tau(\sigma'(j)))(1 - \delta(\sigma(i), \sigma'(j))) + \sum_{\sigma} \lambda(\sigma)(v(\sigma) - v_T(\sigma))^2 + H_{chemo} + H_{AM}$$

$$\Delta H_{chemo(GF)} = -\lambda_{chemo} \cdot (c_i - c_j)$$

$$\Delta H_{AM} = -\vec{\lambda} \cdot \left(\vec{x}_{target} - \vec{x}_{source}\right)$$

The time evolution of simulations in CC3D involves many attempts to copy cell indices between neighboring pixels. On a successful index copy attempt, the volume of the source cell goes up while that of the target cell goes down by one pixel (please see the introduction to the Compucell3D manual).

A Monte Carlo step (MCS) consists of one index copy attempt for each pixel in the cell lattice. Modified Metropolis with Boltzmann acceptance function regulates attempts to copy indices. At any given MCS, if the index copy attempt is successful, the effective energy of the new configuration will be evaluated. If the change in effective energy is negative, then that index copy attempt is considered and implemented, which will be depicted in the next MCS in the simulation. If the change in effective energy is positive, then there is a probability associated with that index copy attempt to happen described by the Boltzmann acceptance function.

$$\mathrm{P} = 1 \quad \text{if } \Delta H < 0$$

$$\mathrm{P} = 1 - \exp\left(\frac{-\Delta H}{T_m}\right) \quad \text{if } \Delta H > 0$$

where ΔH is change in effective energy if the copy occurs and T_m is a parameter describing the amplitude of cell-membrane fluctuations (51).

The first term of effective energy corresponds to contact energies and adhesion. For instance, in the case of model adhesion strengths, when the i,j pixels correspond to the pixels at the boundary/interface of two cancer cells J takes the value 46 in the first term. When the i,j pixels corresponds to pixels at the interface of a cancer cell and laminin-rich ECM $J = 4$ and for the interface between a cancer cell and collagen I (Co1) ECM $J = 46$. The second term in effective energy is the volume

Please cite this article in press as: Prasanna et al., Spatial heterogeneity in tumor adhesion qualifies collective cell invasion, Biophysical Journal (2024), https://doi.org/10.1016/j.bpj.2024.05.005

constraint energy term, which is analogous to the spring energy term. It ensures that the cell volume $v(\sigma)$ does not deviate from the cell's target volume $v_T(\sigma)$. $\lambda(\sigma)$ is like a spring constant that denotes the inverse compressibility of the cell. $v(\sigma)$ of each cancer cell is governed by growth equation (3).

$\Delta H_{chemo(GF)}$ and H_{AM} terms of the current model are specific to cancer cells only in the simulations. $\Delta H_{chemo(GF)}$ enables chemotaxis of cancer cells that represents a biased motility of cells in response to the growth factor (GF) chemical gradient they are exposed to. c_i represents the concentration of the chemical field (GF) at the index-copy target pixel (i) while c_j corresponds to the same at the index-copy source pixel (j). λ_{chemo} is the strength of the chemotaxis that cells respond to. ΔH_{AM} is used to model the forces between the cells. (AM in the subscript corresponds to active motility of the cells.) $(\vec{x}_{target} - \vec{x}_{source})$ is the difference between position vectors of source and target pixels while $\vec{\lambda}$ is the strength and direction of external force between the cells. In the current model, ΔH_{AM} it is used to take into consideration the forces between the cells that give rise to random cell motion. The respective steppable (CellMotility steppable) provides an external force on the center of mass of the cells which changes direction randomly every MCS.

Simulation details of the model

The domain of simulation we constructed is a $100 \times 100 \times 1$ square lattice with a nonperiodic boundary condition consisting of seven different entities that are explained below (3). In the simulations, the lengths and volume dimensions are measured in terms of number of pixels or voxels and the MCS is the unit of time.

Medium

These are unassigned cell types in the background on which the computational model is constructed in the simulation domain.

Cancer cells

These cells are positioned at the center of the simulation surrounded by basement membrane/laminin. There are two types of cancer cells: cancer cell subset 1 (C1), which is indicated by red, and cancer cell subset 2 (C2), which is indicated by yellow. Each cancer cell has a volume of $(4 \times 4 \times 1)$ pixels, and the tumor is a grid of 16 such cancer cells with 8 cells of each type. Only the cancer cells in the simulation have the property to respond to chemical gradients of growth factor, grow, proliferate, and degrade ECM.

BM (laminin-rich ECM)

This cell type corresponds to the thick basal lamina which surrounds and holds together the luminal epithelial cells in the mammary duct. In simulations, this is represented by a two-layered, blue-colored annular basement membrane binding the cancer cells together and separating them from Co1/ECM (3).

Co1

These cells mimic the fibrillar ECM surrounding the tumor. Cancer cells degrade Co1 and invade through it.

C_lysed

This cell type is used in an intermediate step during matrix degradation and regeneration. The dynamics of reaction-diffusion of the chemicals secreted by cancer cells allow for the degradation of BM and Co1 matrix cells. Upon meeting certain criteria for degradation, the BM or Co1 cell type of a particular cell becomes C_lysed, although retaining the shape and size of the cell. These cells track the MCSs from their individual degradation event and transform it into newly synthesized matrix cells after 20 MCSs.

NC1

This cell type is intended to mimic the "cancer matrisome," the newly synthesized matrix cells are denoted as NC1. These cells are almost identical to Co1 in their behavior and can undergo further degradation to become C_lysed and subsequently after 20 MCSs, would become NC1 again.

Reaction-diffusion, growth, and proliferation equations

The growth of cancer cells is governed by the ODE.

$$\frac{dV}{dt} = G\{g.p + [GF].q\}$$

where V is the volume of cancer cell, g is the measure of nutrient availability, [GF] is the concentration of growth factor (GF) at the center of mass of the cancer cell, p, q are constants, G is the growth rate coefficient.

Although our multiscale model deploys reaction-diffusion-based interactive dynamics of soluble matrix metalloproteinases and their inhibitors, this has not been analyzed formally in this manuscript and readers are encouraged to refer to our previous paper for further details on this aspect of the model description (3).

Starting spatial patterns and heterogeneity

The spatial heterogeneity in tumors at the beginning of the simulation was represented through the following five spatial patterns: namely low HI I, low HI II, mid HI I, mid HI II, and high HI. Besides them, spatial patterns intermediate to low and mid HI, intermediate to mid and high HI, and a special case (Fig. 7) were considered.

Spatial heterogeneity at the cellular level is considered as the ratio of number of dissimilar cells surrounding the given cell to the total number of cells surrounding it. Summing up these ratios calculated for all cells of one subtype in each spatial pattern yields the heterogeneity index (HI) of that cell subtype. The HI of both cell subtypes is considered as the HI of the spatial pattern. In the case of unequal HI between cell subtypes, the average of both the values is taken as the HI of the spatial pattern. In the current definition of HI only first-order neighbors, i.e., adjacent cells that share a common edge, are considered as surrounding cells. Therefore, it shall be 4 for an interior cell and 3 for a peripheral cell, except for the corner cells. The corner cells will have 2 surrounding cells.

$$\mathrm{HI} = \sum_{\substack{\forall \text{ cells} \\ of\ one\ \text{subtype}}} \left(\frac{number\ of\ dissimilar\ cells}{total\ number\ of\ surrounding\ cells} \right)$$

The HI calculations for red cells in spatial patterns in (Fig. 1 *C*) starting from topmost left and traversing clockwise are shown below.

Low HI I and II: low HI $= \left(\frac{1}{3}\right) + \left(\frac{1}{4}\right) + \left(\frac{1}{4}\right) + \left(\frac{1}{3}\right) + \left(\frac{0}{2}\right) + \left(\frac{0}{3}\right) + \left(\frac{0}{3}\right) + \left(\frac{0}{2}\right) = 1.167$

Low HI < HI < mid HI: HI $= \left(\frac{2}{3}\right) + \left(\frac{4}{4}\right) + \left(\frac{2}{4}\right) + \left(\frac{1}{3}\right) + \left(\frac{0}{2}\right) + \left(\frac{1}{3}\right) + \left(\frac{0}{3}\right) + \left(\frac{0}{2}\right) = 2.833$

Mid HI I and II: mid HI $= \left(\frac{1}{2}\right) + \left(\frac{1}{3}\right) + \left(\frac{1}{3}\right) + \left(\frac{1}{2}\right) + \left(\frac{2}{3}\right) + \left(\frac{2}{4}\right) + \left(\frac{2}{4}\right) + \left(\frac{2}{3}\right) = 4$

Mid HI < HI < high HI: HI $= \left(\frac{3}{3}\right) + \left(\frac{2}{2}\right) + \left(\frac{4}{4}\right) + \left(\frac{3}{3}\right) + \left(\frac{3}{3}\right) + \left(\frac{1}{2}\right) + \left(\frac{1}{3}\right) + \left(\frac{2}{3}\right) = 6.5$

High HI: high HI $= \left(\frac{2}{2}\right) + \left(\frac{3}{3}\right) + \left(\frac{3}{3}\right) + \left(\frac{2}{2}\right) + \left(\frac{3}{3}\right) + \left(\frac{4}{4}\right) + \left(\frac{4}{4}\right) + \left(\frac{3}{3}\right) = 8$

Scaling the above values of HI from 0 to 1 and rounding off to second decimal, we get the new HI values as

Low HI $= (1.167/8) = 0.15$

Low HI < HI < mid HI $= (2.833/8) = 0.35$

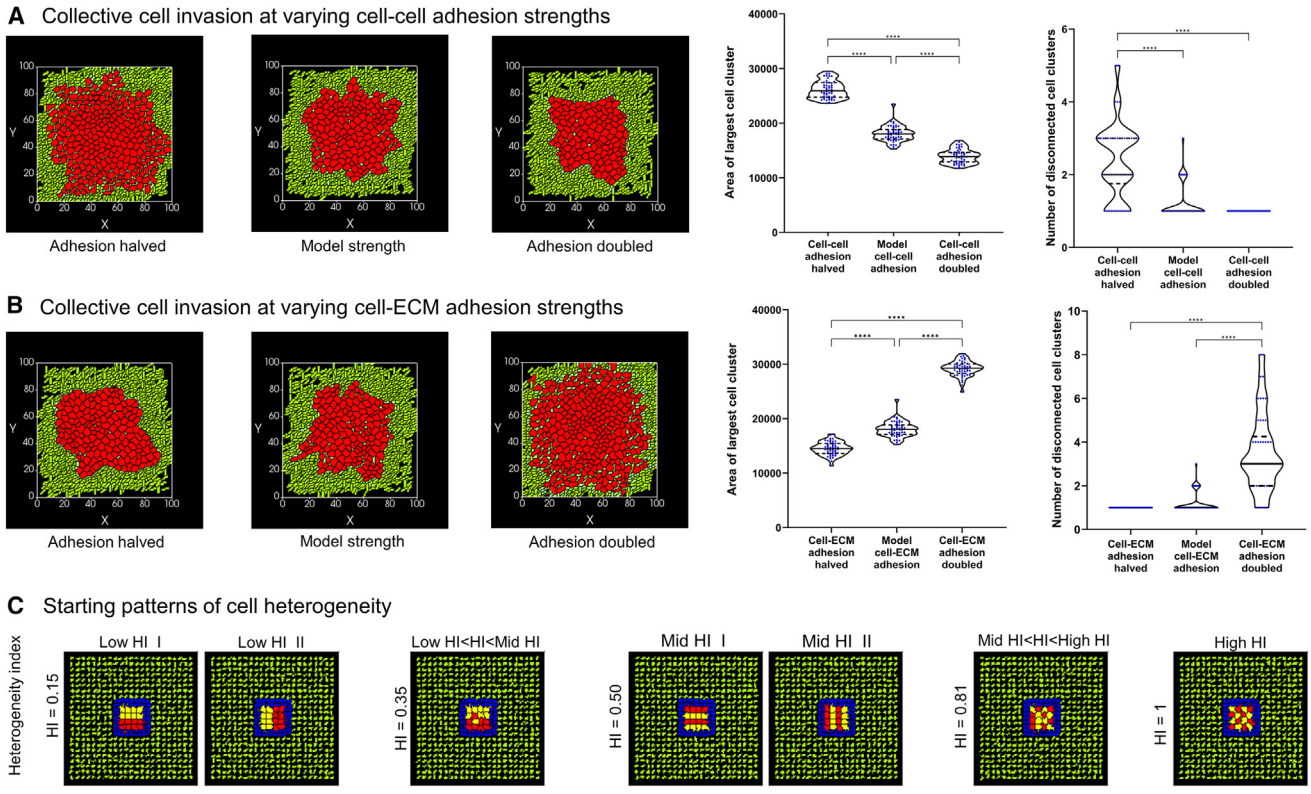

FIGURE 1 Introduction to the computational framework for the study of regulation of collective cancer invasion by spatial cell patterns with varying cellular and matrix adhesion. (*A*) Phenotypes of tumor populations of cells (in *red*) at the end of simulations run (1200 MCSs), wherein cells had model cell-cell adhesion strength (that had been shown to give rise to collective invasion in Pramanik et al. (3); *center*), with half the model cell-cell adhesion strength (*left*) and with double the model cell-cell adhesion strength (*right*). Violin plots with medians for area of largest cell cluster (used as a measure of collective invasion) and number of disconnected cell clusters (used as a measure of dispersed invasion) for 50 simulations each for the three cell-cell adhesion strengths are shown on the right. (*B*) Phenotypes of tumor populations of cells (in *red*) at the end of simulations run (1200 MCSs), wherein cells had model cell-ECM adhesion strength (that had been shown to give rise to collective invasion in Pramanik et al. (3); *center*), with half the cell-ECM adhesion strength (*left*) and with double the cell-ECM adhesion strength (*right*). Violin plot with medians for area of largest cell cluster (used as a measure of collective invasion) and number of disconnected cell clusters (used as a measure of dispersed invasion) for 50 simulations each for the three cell-ECM adhesion strengths are shown on the right. (*C*) Phenotypes of tumor populations at the beginning of simulations comprising two types of cancer cells (colored *yellow* and *red*) with distinct cell-cell or cell-ECM adhesion strengths, arranged in spatial patterns with an increasing degree of heterogeneity index (HI) (see appropriate section in the materials and methods for definition) from left to right (*leftmost*: consecutive horizontal and vertical patterns with HI = 0.15; consecutive pattern with a single-cell pair swap with HI = 0.35; alternate horizontal and vertical patterns with HI = 0.50; pattern with a single-cell pair swap with HI = 0.81; checkered pattern with HI = 1) Statistical significance for the measurements in the simulations was computed using one-way ANOVA with Tukey-Kramer post hoc comparisons. Significance (p value) is represented as *, where $*p \leq 0.05$, $**p \leq 0.01$, $***p \leq 0.001$, and $****p < 0.0001$. To see this figure in color, go online.

Mid HI = (4/8) = 0.5
Mid HI < HI < high HI = (6.5/8) = 0.81
High HI = (8/8) = 1

Scaled HI value for specific case pattern = (0.4167 + 0.29167)/2 = 0.35, where 0.4167 is the HI of the red subset of cells and 0.29167 is the HI of the yellow subset of cells.

Statistical analysis

All CC3D simulation screenshots at 1200 MCSs were taken (1000 MCSs for simultaneous variation of both cell-cell and cell-ECM cases) to do image quantification analysis in MATLAB. Considering that the cellular dynamics incorporated in our model are stochastic in nature and to ensure a large sample size for statistical analysis, 50 replicates of the cases were carried out. For statistical analysis, one-way ANOVA was performed followed by the Tukey-Kramer test as a post hoc analysis in GraphPad on the heterogeneous and homogeneous simulations of every case to draw inferences and conclusions. Significance (p value) is represented as *, where $*p \leq 0.05$, $**p \leq 0.01$, $***p \leq 0.001$, and $****p < 0.0001$.

RESULTS

Impact of inter-subset and intra-subset cell-cell adhesion spatial heterogeneity on CCI

We began our study by examining the effects of variation in adhesion strengths on invasion in our framework under conditions when such strengths have been kept uniform across the cell population ("homogeneous pattern") (Fig. 1). Our previous work had identified adhesion strengths (we refer to them

Please cite this article in press as: Prasanna et al., Spatial heterogeneity in tumor adhesion qualifies collective cell invasion, Biophysical Journal (2024), https://doi.org/10.1016/j.bpj.2024.05.005

for the sake of convenience in this paper as "model" adhesion strengths) at which we had observed CCI (3). CCI and DCI were assessed as before by measuring the area of the largest connected cluster of cells, and the number of disconnected cells or their clusters, respectively (see Fig. S1 for a description of image analysis and a compendium of parameter values employed in the model). When cell-cell adhesion strength was halved or doubled, the cell population with homogeneous adhesion pattern showed 1.45-fold higher and 0.77-fold lower CCI, respectively, consistent with a frequently observed role in experiments of intercellular homotypic adhesion mediators as suppressors of metastasis (23) (Fig. 1 *A*; ANOVA $p < 0.0001$). We also confirmed that the dependence of CCI on cell-cell adhesion for a wider range of values of the latter (Fig. S2; ANOVA $p < 0.0001$). High adhesion to fibrillar ECM such as Co1 through integrins has been shown to be important for CCI (4,24). In support, when the adhesion strength between cancer cells and stromal ECM (in most epithelial tissues, the predominant ECM in stroma is Co1) was halved or doubled, the cell population with homogeneous pattern showed 0.80-fold lower and 1.61-fold higher CCI, respectively (Fig. 1 *B*; ANOVA $p < 0.0001$; Fig. S2 establishes the same for a wider set of cell-ECM adhesion strengths, ANOVA $p < 0.0001$). DCI, as measured through disconnects in motile cells or clusters, was marginally altered for one of the subcases, while it was significant for the other subcase (Fig. 1 *A*, *rightmost graph*; Kruskal-Wallis test $p < 0.0001$), (Fig. 1 *B*, *rightmost graph*; Kruskal-Wallis test $p < 0.0001$). These results are consistent with experiments that posit an antagonistic interplay between cell-ECM and cell-cell adhesive interactions that drive the disaggregation of cellular clusters leading to invasion (25).

We subsequently moved to heterogeneous pattern cases, wherein the above-mentioned adhesion strengths can be observed to spatially vary across a cell population (in this article, red- and yellow-colored cells represent cells with distinct adhesion strengths). We quantified this variation through the heterogeneity index (HI), which measures the mean of immediate dissimilar cell neighbors for each cell in the starting cell population (Fig. 1 *C*, see appropriate section in the materials and methods for definition). To explore the effects on invasion across the HI, we examined distinct spatial patterns, which we call low HI I and II (here, the adhesion strengths have been kept the same for two consecutive rows of red or yellow cells resembling a tumor with two distinct well-sorted cell populations), mid HI I and II (here, the adhesion strengths alternate between rows of red and yellow cells resembling a tumor with two distinct but moderately intermingled cell populations), and finally a high HI pattern (here, the adhesion strength alternates between two consecutive cells within the population resembling a tumor with prolific cell state mingling). The rationale for examining the consecutive or alternating arrangements along two axes, and hence two versions each for low and mid HI, was to discount any confounding effects by the alignment of fibrillar ECM (from bottom-left to top-right of the simulation frame) on the symmetry of the migrating cell pattern. In addition to these symmetric patterns, we also swapped a pair of red and yellow cells each for the low HI and high HI cases to evince asymmetric patterns whose HI therefore lies intermediate between low and mid HI patterns, and mid HI and high HI patterns, respectively.

To examine the role of heterogeneity in cell-cell adhesion in CCI, we first carried out simulations on progressively intermingled populations, wherein the two cellular subsets showed adhesion to their own respective subset cell type that were half and double the model adhesion strength (i.e., yellow cells having cell-cell adhesion half of the model cell-cell adhesion and red cells having cell-cell adhesion double that of the model cell-cell adhesion). In addition, for each simulation we varied the inter-subset cell adhesion strength from half to double the model cell-cell adhesion strength. We observed that, in the context of lower inter-subset adhesion strength (Fig. 2 *A*; see also Videos S1 and S2), i.e., when the two populations were least adhered to each other, the CCI shown by patterns increased in direct proportion with their HI (Fig. 2 *B*; ANOVA $p < 0.0001$, significant differences observed between patterns with widely diverged HI through post hoc comparisons, e.g., 1.07-fold between the high HI and low HI I pattern). Observing the population phenotypes at the end of simulations showed that low inter-subset adhesion strength ensured that irrespective of how intermingled they were at the beginning of the simulation, the subsets eventually sorted out from each other. None of the patterns under such contexts showed any notable dispersion (Fig. 2 *C*). We also observed that the ratio between the CCI pertaining to the high HI and low HI I pattern cases increased proportionately from 1.07-fold to 1.12- and 1.13-fold as the fold change of adhesion strength was increased from 4-fold (half and double) to 9-fold (one-third and triple), and 16-fold (one-fourth and quadruple) respectively, suggesting that our observations were consistent across a diverse set of differences in adhesion strengths of the subsets (Fig. 2 *D*; two-tailed Student's *t*-test $p < 0.0001$). To ascertain that the invasion involved both cell division events and migration of cells within tumoroid masses, we performed cell tracking and traced out the temporal fates of three cells at the beginning of the simulations, through their migration trajectories, interspersed by cell division events (Fig. S3; Video S3).

The relationship between CCI and HI gets switched when inter-subset adhesion strength is assigned a high value (Fig. 3 *A*; see also Videos S4 and S5), i.e., when the two populations strongly adhered to each other: here, invasion of patterns showed an inversely proportional relationship with their HI (Fig. 3 *B*; ANOVA $p < 0.0001$, significant differences observed between patterns with widely diverged HI through post hoc comparisons, e.g., 0.91-fold between the high HI and low HI I pattern). In addition, we observed that the high inter-subset adhesion strength engendered strong intermingling of subsets at the end of simulations carried out for

Please cite this article in press as: Prasanna et al., Spatial heterogeneity in tumor adhesion qualifies collective cell invasion, Biophysical Journal (2024), https://doi.org/10.1016/j.bpj.2024.05.005

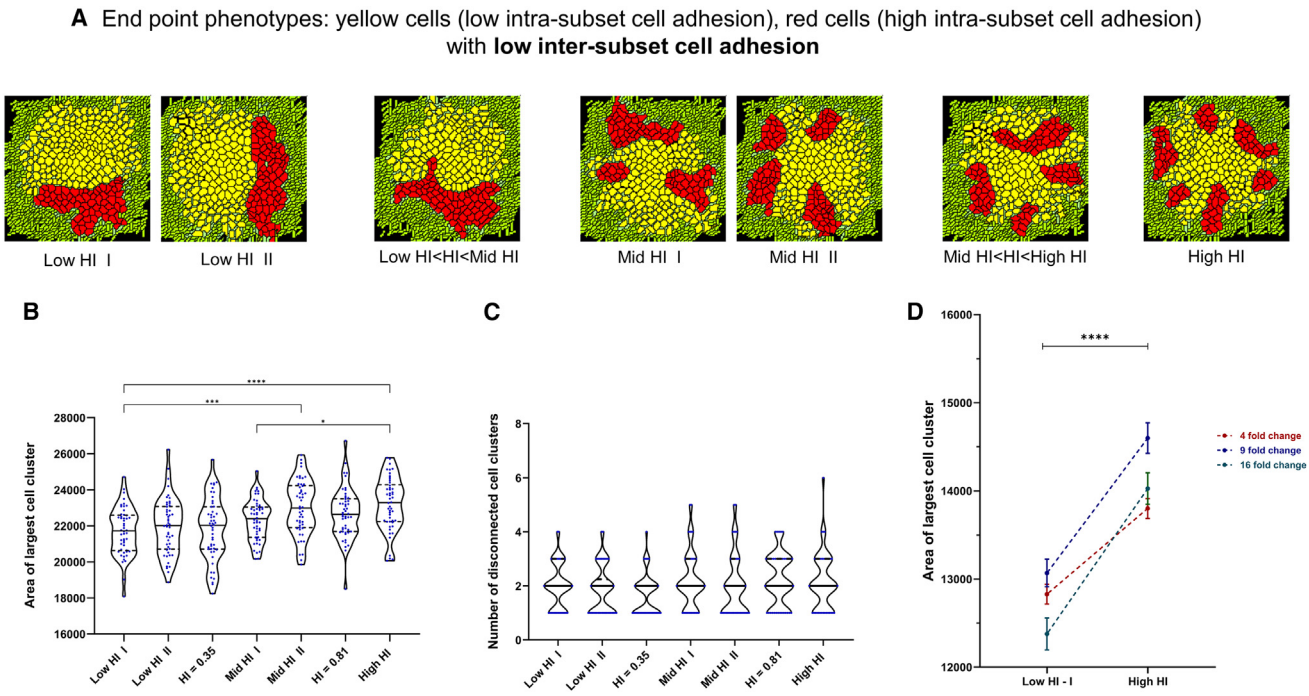

FIGURE 2 Collective invasion in tumor populations with heterogeneous intra-subset cell adhesion and low inter-subset cell adhesion. (*A*) Endpoint (1200 MCSs) phenotypes of tumor populations with progressively increasing HI values of starting patterns with yellow cells (low intra-subset adhesion), red cells (high intra-subset adhesion), and low inter-subset adhesion (see also Videos S1 and S2). (*B*) Violin plot with median of area of largest cell cluster (used as a measure of collective cell invasion) for 50 simulations each for patterns from low to high HI values. Statistical significance for the measurements in the simulations was computed using one-way ANOVA with Tukey-Kramer post hoc comparisons. Significance (p value) is represented as *, where $*p \leq 0.05$, $**p \leq 0.01$, $***p \leq 0.001$, and $****p < 0.0001$. (*C*) Violin plot with median of the number of disconnected cell clusters (used as a measure of dispersed invasion) for 50 simulations each for patterns from low to high HI values. (*D*) Graph showing the increase in the collective invasion of tumors with high HI pattern compared with low HI pattern when fold change of cell-cell adhesion strength between subsets is 4-fold (*red*), 9-fold (*blue*), and 16-fold (*green*). Statistical significance for the measurements in the simulations at 800 MCSs was computed using two-tailed Student's t-test. Significance (p value) is represented as *, where $*p \leq 0.05$, $**p \leq 0.01$, $***p \leq 0.001$, and $****p < 0.0001$. To see this figure in color, go online.

populations with varying degrees of HI. This implies that adhesion-heterogeneous tumor populations that are well intermingled will collectively invade better only in the context of weak interniche adhesion, i.e., when heterotypic cell-cell adhesion is sparse. Under strong interniche adhesive contexts, coarsely intermingled tumor populations invade better. As in Fig. 2 *C*, there was very little DCI shown by such migrating cell populations (Fig. 3 *C*). Consistent with what we observed in Fig. 2 *D*, the ratio between the CCI pertaining to the high HI and low HI I pattern cases decreased proportionately from 0.93-fold to 0.91- and 0.88-fold as the fold change of adhesion strength was increased (Fig. 3 *D*; two-tailed Student's t-test $p < 0.0001$).

Influence of heterogeneous cell-ECM adhesion on the collective invasion phenotype

We next investigated the invasion of heterogeneous cell patterns under different cell-ECM adhesion strengths (Fig. 4 *A*; see also Videos S6 and S7), while considering no heterogeneity in cell-cell adhesion. For simulations in which the two subpopulations showed halved and doubled model cell-ECM adhesion strengths, respectively (i.e., yellow cells having cell-ECM adhesion half of the model cell-ECM adhesion and red cells having cell-ECM adhesion double that of model cell-ECM adhesion), we found a progressive increase in CCI as the HI in cell-ECM adhesion strength was increased (Fig. 4 *B*; ANOVA $p < 0.0001$, significant differences observed between patterns with widely diverged HI through post hoc comparisons, e.g., 1.13-fold between the high HI and low HI pattern). We observed only insignificant variations in DCI (Fig. 4 *C*). The population phenotypes at the end of the simulations showed that the intermingling of subsets was broadly recapitulative of their starting pattern (Fig. 4 *A*). We also observed that the ratio between the CCI pertaining to the high HI and low HI I pattern cases increased proportionately from 1.09-fold to 1.18- and 1.20-fold as the fold change of cell-ECM adhesion strength was increased (Fig. 4 *D*; two-tailed Student's t-test $p < 0.0001$).

Incorporating heterogeneity in both cell-cell and cell-ECM adhesion components

So far, we examined the effects of heterogeneity in adhesion strengths of cells with each other or with their surrounding ECM separately from each other. However, signaling

Please cite this article in press as: Prasanna et al., Spatial heterogeneity in tumor adhesion qualifies collective cell invasion, Biophysical Journal (2024), https://doi.org/10.1016/j.bpj.2024.05.005

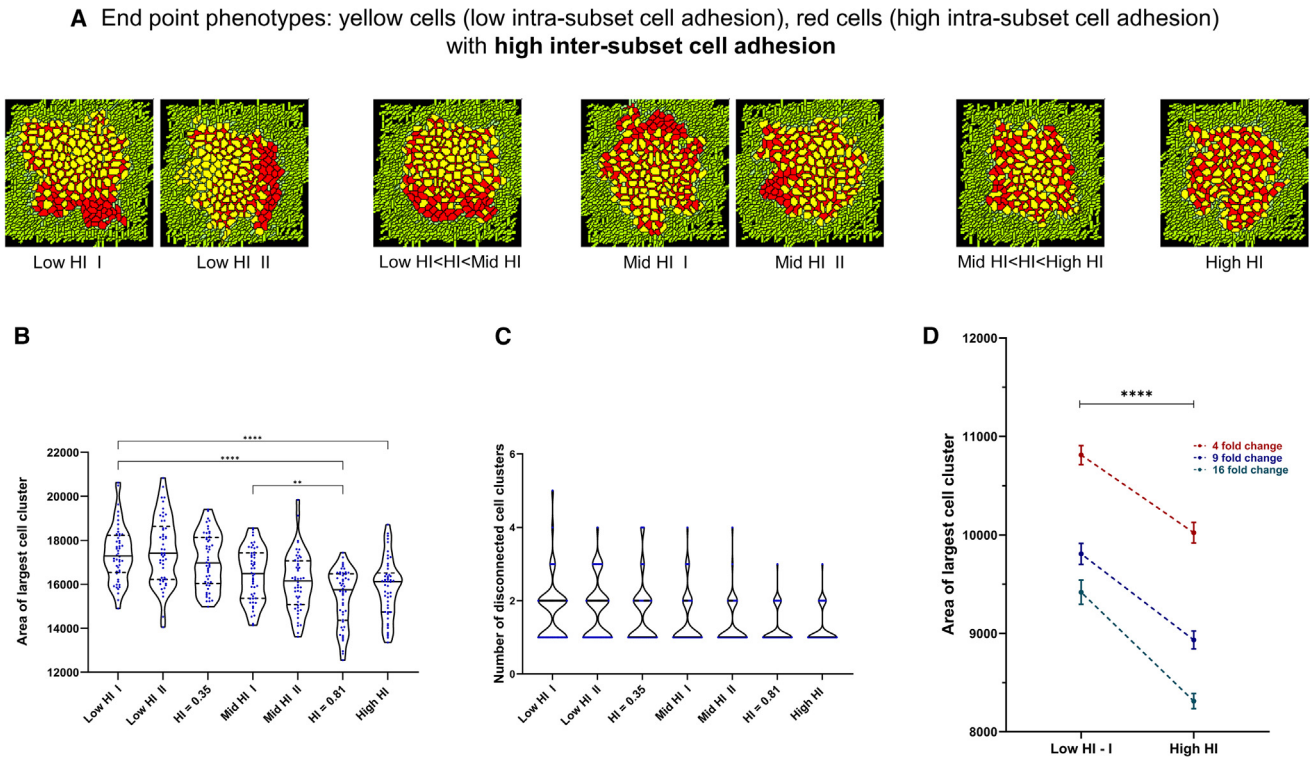

FIGURE 3 Collective invasion in tumor populations with heterogeneous intra-subset cell adhesion and high inter-subset cell adhesion. (*A*) Endpoint (1200 MCSs) phenotypes of tumor populations with progressively increasing HI values of starting patterns with yellow cells (low intra-subset adhesion), red cells (high intra-subset adhesion), and high inter-subset adhesion (see also Videos S4 and S5). (*B*) Violin plot with median of the area of largest cell cluster (used as a measure of collective cell invasion) for 50 simulations each for patterns from low to high HI values. Statistical significance for the measurements in the simulations computed using one-way ANOVA with Tukey-Kramer post hoc comparisons. Significance (p value) is represented as *, where $*p \leq 0.05$, $**p \leq 0.01$, $***p \leq 0.001$, and $****p < 0.0001$. (*C*) Violin plot with median of the number of disconnected cell clusters (used as a measure of dispersed invasion) for 50 simulations each for patterns from low to high HI values. (*D*) Graph showing the decrease in the collective invasion of tumors with high HI pattern compared with low HI pattern when fold change of cell-cell adhesion strength between subsets is 4-fold (*red*), 9-fold (*blue*), and 16-fold (*green*). Statistical significance for the measurements in the simulations at 800 MCSs was computed using two-tailed Student's *t*-test. Significance (p value) is represented as *, where $*p \leq 0.05$, $**p \leq 0.01$, $***p \leq 0.001$, and $****p < 0.0001$. To see this figure in color, go online.

alterations associated with tumorigenesis cross-link such traits allowing them to combine to shape phenotypes. For example, EMT seen in cancer cells is associated both with a depletion in cell-cell adhesion and an increase in matrix adhesion (26,27). How do such associative changes in adhesion strengths regulate invasion across a tumor population? To answer this question, we first carried out simulations, wherein CCI and DCI were assessed in homogeneous cellular populations with variable levels of both adhesion types (Fig. 5 *A*). Unsurprisingly, cells with stronger cell-cell adhesion but weaker cell-ECM adhesion (double and half of the model adhesion strengths, respectively; resembling stereotypically strong epithelial states) exhibited poor CCI (0.64-fold lower in the epithelial state compared with control; Fig. 5 *B*; ANOVA $p < 0.0001$, significant differences observed between patterns through post hoc comparisons). On the other hand, populations with weaker cell-cell adhesion and stronger ECM adhesion (resembling stereotypically strong mesenchymal states), collectively invaded further but also dispersed into the surrounding ECM as discrete clusters (1.99-fold higher CCI and 6.2-fold higher DCI in the mesenchymal state compared with control; Fig. 5, *B* and *C*; in Fig. 5 *C*, ANOVA $p < 0.0001$, significant differences observed between the mesenchymal pattern and control and epithelial patterns assessed through post hoc comparisons) as has been observed in experiments (28).

Heterogeneity in cellular and histological phenotypes driven by nongenetic, genetic, and microenvironmental cues is the norm of tumor populations (7,29). Among the axes of heterogeneity, there is mounting evidence for the concurrent presence within cancer populations of cellular phenotypes across the epithelial to mesenchymal spectrum (30,31). To test the consequences of the spatial arrangement of a heterogeneous population of epithelial and mesenchymal cells on their invasion, we conducted simulations of patterns with different HI values and with high inter-subset cell adhesion strength (Fig. 6 *A*). We observed an inversely proportional relationship between HI values and the extent of CCI (Fig. 6 *A left graph*; ANOVA $p < 0.0001$, significant differences observed between patterns with widely diverged HI through post hoc comparisons, e.g., 0.9-fold difference in high HI and low HI patterns

Please cite this article in press as: Prasanna et al., Spatial heterogeneity in tumor adhesion qualifies collective cell invasion, Biophysical Journal (2024), https://doi.org/10.1016/j.bpj.2024.05.005

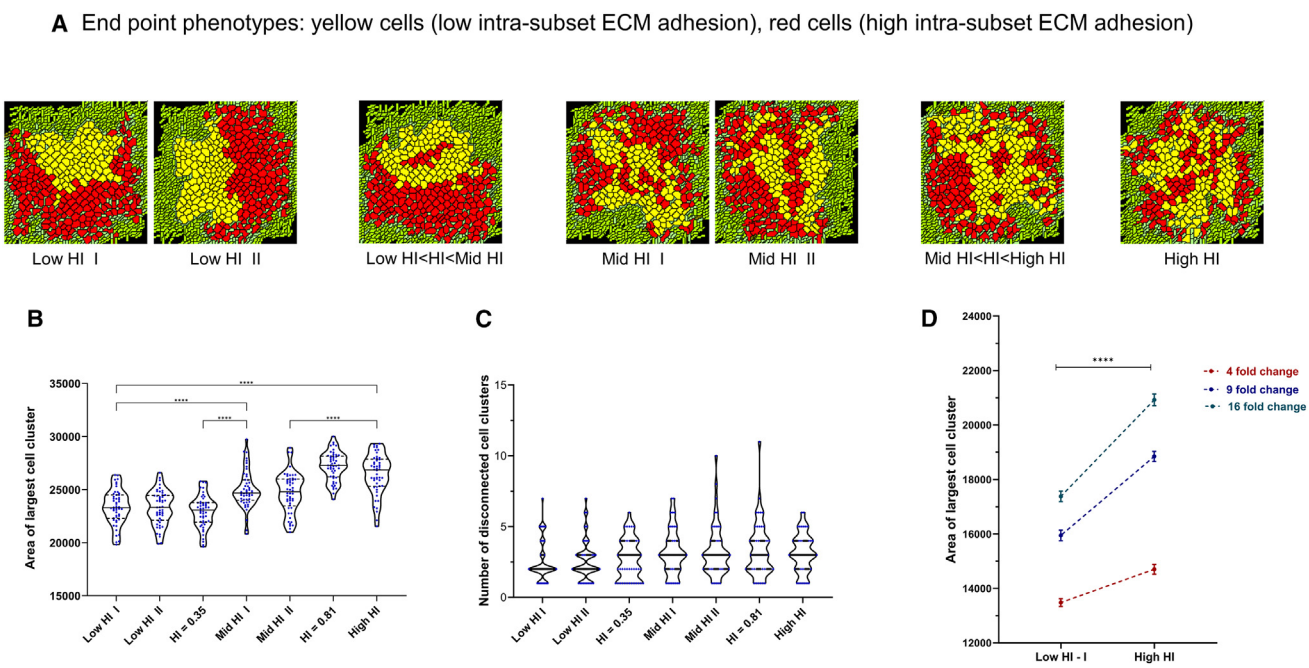

FIGURE 4 Collective invasion in tumor populations with heterogeneous intra-subset cell-ECM adhesion. (*A*) Endpoint (1200 MCSs) phenotypes of tumor populations with progressively increasing HI values of starting patterns with yellow cells (low intra-subset cell-ECM adhesion) and red cells (high intra-subset cell-ECM adhesion) (see also Videos S6 and S7). (*B*) Violin plot with median of the area of largest cell cluster (used as a measure of collective cell invasion) for 50 simulations each for patterns from low to high HI values. Statistical significance for the measurements in the simulations was computed using one-way ANOVA with Tukey-Kramer post hoc comparisons. Significance (p value) is represented as *, where *$p \leq 0.05$, **$p \leq 0.01$, ***$p \leq 0.001$, and ****$p < 0.0001$. (*C*) Violin plot with median of the number of disconnected cell clusters (used as a measure of dispersed invasion) for 50 simulations each for patterns from low to high HI values. (*D*) Graph showing the increase in the collective invasion of tumors with high HI pattern compared with low HI pattern when fold change of cell-cell adhesion strength between subsets is 4-fold (*red*), 9-fold (*blue*), and 16-fold (*green*). Statistical significance for the measurements in the simulations at 800 MCSs was computed using two-tailed Student's *t*-test. Significance (p value) is represented as *, where *$p \leq 0.05$, **$p \leq 0.01$, ***$p \leq 0.001$, and ****$p < 0.0001$. To see this figure in color, go online.

for CCI). Moreover, regardless of HI values, all endpoint simulations showed a strong intermingling of epithelial and mesenchymal cells. In contrast, when inter-subset cell adhesion strength is kept low, HI values show a directly proportional relationship with the extent of CCI (Fig. 6 *B left graph*; ANOVA $p < 0.0001$, significant differences observed between patterns with diverged HI through post hoc comparisons, e.g., 1.16-fold difference in high HI and low HI patterns for CCI). In these simulations, regardless of HI values, the two populations got sorted out efficiently. For high inter-subset adhesion strengths, post hoc comparisons showed little difference in DCI between different HI patterns. However, a progressive increase in DCI was observed in the low inter-subset cell adhesion case, where high HI patterns showed the strongest dispersion compared with all other patterns (-ANOVA $p < 0.0001$, significant differences observed between patterns with diverged HI through post hoc comparisons).

We next asked if assessing the HI of initial tumor population pattern is sufficient to predict the relative extent of collective invasion in heterogeneous cancer cell populations. To our surprise, we observed patterns with relatively lower HI (for cell-ECM heterogeneous adhesion case HI = 0.35 with ECM-adherent red cells at periphery), which showed higher CCI (1.04-fold higher than the pattern with HI = 1; Fig. 7 *B*; ANOVA $p < 0.0001$) but insignificantly different DCI (Fig. 7 *C*; Kruskal-Wallis test $p < 0.0001$). These patterns were characterized by a relatively greater partitioning of cells with higher adhesion to collagen to the radially outer edge of the tumor population. Interestingly, the reverse pattern (with the same HI of 0.35 but with ECM-adherent red cells in interior) showed much lower CCI (0.78- and 0.82-fold lower than the patterns with HI = 0.35 and 1, respectively; Fig. 7 *A–C*). Cellular arrangements with a radially outward partitioning of ECM-adhesive cells have especially been shown to be associated with high migrative efficiency in experiments with cocultures of aggressive breast cancer cells comprising niches that are distinct in their cell-ECM strengths (15). Our observations therefore suggest that cancer cells with greater ability to adhere to stromal fibrillar collagens contribute further to CCI when they are spatially well distributed across the tumor, but especially to the outer edge, where they can exert their adhesive effects on the neighboring ECM more efficiently than other patterns.

DISCUSSION

Tumors show heterogeneous signatures across molecular and cellular scales. Clonal populations may exist with

Please cite this article in press as: Prasanna et al., Spatial heterogeneity in tumor adhesion qualifies collective cell invasion, Biophysical Journal (2024), https://doi.org/10.1016/j.bpj.2024.05.005

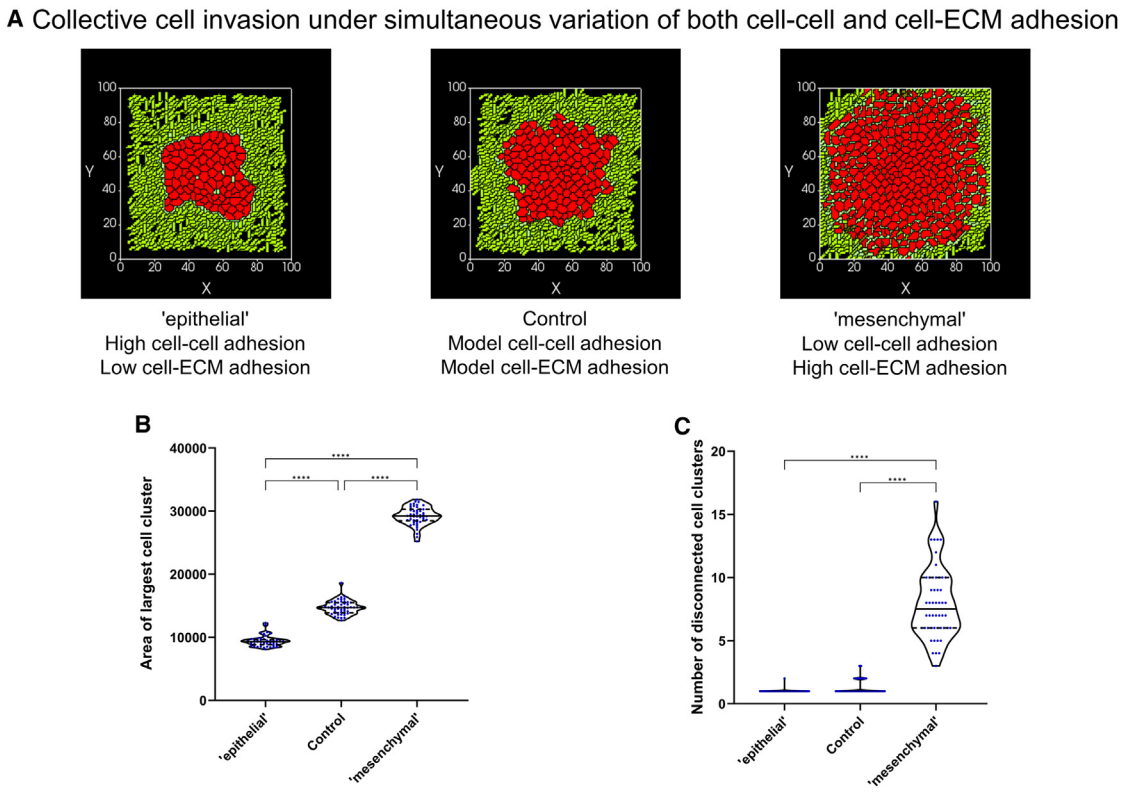

FIGURE 5 Invasion upon simultaneous variation of both cell-cell and cell-ECM adhesion strengths. (*A*) Phenotypes of tumor populations of cells (in *red*) at the end of simulations run (1000 MCSs), wherein cells had model cell-cell and cell-ECM adhesion strength (*center*; control), with double of model cell-cell and half of model cell-ECM adhesion strength (*left*; "epithelial"), and with half of model cell-cell and double of model cell-ECM adhesion strength (*right*; "mesenchymal"). (*B*) Violin plot with median of area of largest cell cluster for epithelial, control (collective invasion), and mesenchymal (multimodal mode of invasion). (*C*) Violin plot with median of number of disconnected cell clusters for epithelial, control, and mesenchymal. Statistical significance for the measurements in the simulations was computed using one-way ANOVA with Tukey-Kramer post hoc comparisons. Significance (p value) is represented as *, where $*p \leq 0.05$, $**p \leq 0.01$, $***p \leq 0.001$, and $****p < 0.0001$. To see this figure in color, go online.

distinct single-nucleotide and copy-number variations (32), protein expression (12), cellular phenotypes (33), and histopathological features (34). However, the extent to which distinct heterogeneous behaviors correspond spatially across scales is yet to be well understood (although see (34) for a demonstration of a correspondence between variation in nuclear morphology and genomic instability). Various reports on spatial heterogeneity in primary tumors report a gradient of EMT such that the leading edge is relatively more mesenchymal (35–37). Such observations have been explained by computational models invoking a diffusible EMT-inducing signal such as TGF-β, known to be secreted by stromal cells (38); however, these studies do not investigate the functional contributions of spatial heterogeneity in tumor progression. Further, in vitro studies on CCI highlight that this EMT gradient is rather dynamic, given the exchange of leader and follower cells in a coordinated manner (39,40). Thus, elucidating the functional roles of spatial heterogeneity becomes crucial.

While a series of elegant studies show spatial heterogeneity in clonal populations as confounding management and potentiating metastasis and mortality (34,41,42), they do not explicitly study the consequences of the degree of intermingling between two or more heterogeneous signature-expressing clones. The reason for this could be the difficulty in inferring cell behavioral traits from (multi)omic expressions assayed through sequencing studies. Studying lung adenocarcinoma, Wu et al. have broken fresh ground by demonstrating two distinct diversification patterns, which they call clustered and random geographic diversification patterns (12). These two correspond broadly to our two ends in the spectrum of HI patterns. They show that the random pattern was more deleterious in its association with disease recurrence and mortality. Our simulations provide a formal and contextual basis for such observation. It also allows us to propose that the association of such a random diversification pattern with cancer cell invasion is facilitated under conditions of lower cell-cell adhesion between heterogeneous niches. Under higher adhesion conditions, a random pattern may have opposite consequences.

Recent studies on primary tumor explants show heterogeneity in rigidity across multicellular and cellular scales, with soft motile cells surrounding islands of immotile stiff tumor epithelia. The relation between cell-cell adhesion and

Please cite this article in press as: Prasanna et al., Spatial heterogeneity in tumor adhesion qualifies collective cell invasion, Biophysical Journal (2024), https://doi.org/10.1016/j.bpj.2024.05.005

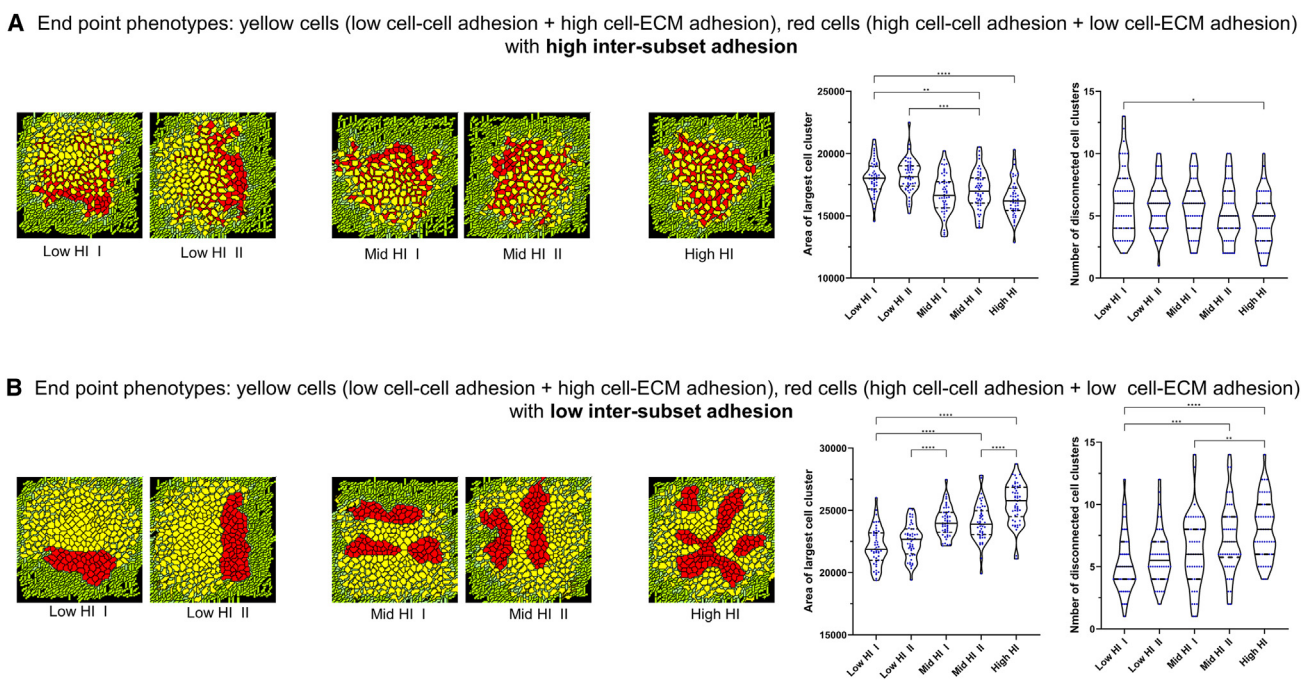

FIGURE 6 Invasion in tumor populations with heterogeneity in intra-subset cell adhesion and cell-ECM adhesion. (*A*) Endpoint (1000 MCSs) phenotypes of tumor populations with progressively increasing HI values of starting patterns with yellow cells (low intra-subset cell adhesion and high cell-ECM adhesion) and red cells (high intra-subset cell adhesion and low cell-ECM adhesion) with high inter-subset cell adhesion. Violin plots with medians for area of largest cell cluster and number of disconnected cell clusters for low, mid, and high HI value spatial patterns on the right. (*B*) Endpoint (1000 MCSs) phenotypes of tumor populations with progressively increasing HI values of starting patterns with yellow cells (low intra-subset cell adhesion and high cell-ECM adhesion) and red cells (high intra-subset cell adhesion and low cell-ECM adhesion) with low inter-subset cell adhesion. Statistical significance for the measurements in the simulations was computed using one-way ANOVA with Tukey-Kramer post hoc comparisons. Significance (p value) is represented as *, where $*p \leq 0.05$, $**p \leq 0.01$, $***p \leq 0.001$, and $****p < 0.0001$. To see this figure in color, go online.

rheological behaviors of tissues and tumors is driven by reciprocal effects of substrata rigidity and organization and expression of cell adhesion proteins and cytoskeletal regulators (43,44). Under non-compliant confining conditions, cancer cells have been observed to show an elevation in cadherin presentation on the cell surface (45), which induces proliferation in such populations. Whether this may influence the intermingling between soft and rigid tumor cells remains unclear. Although our simulations do not impose rheological properties onto cells, we do observe that the initial patterning can be significantly reversed or retained, suggesting active intermingling migration or the lack of it depending on the context. Especially under conditions of low inter-niche adhesion, or under conditions wherein niches with greater ECM adhesion are broadly distributed across the exterior of the tumor, we see rearrangements that reverse the "salt-and-pepper" arrangement of cells (under high HI) to a pattern at the end of simulations, wherein there is significant sorting of cells within relatively homogeneous niches. What was striking in our simulations was that changing either cell-ECM or cell-cell adhesion separately increased invasion but quantitatively, while retaining the collective nature. However, combinatorial alterations led to a qualitative shift in behavior from collective to dispersed (within the surrounding ECM) behavior. This potentially explains why the transition from epithelial character to mesenchymal requires cells to cross-regulate cytoskeletal elements that mediate adhesion to ECM substrata (such as integrins) while also depleting cell-cell adhesion mediators (such as E-cadherin). Future efforts incorporating this biochemical cross-regulation between integrins and E-cadherin can offer a more complete picture of how changes in both cell-cell adhesion and cell-ECM adhesion are achieved during EMT/mesenchymal to epithelial transition (46).

Despite the predictive power of our framework, we would like to highlight the latter's limitations. Our assays are still in a two-dimensional computational space, due mostly to the restraint in computational power required to have a three-dimensional ECM fiber network. Our framework is also not amenable to the direct incorporation of mechanical properties that play an important role in cell-ECM interactions. Third, the consequences of genomic and transcriptional heterogeneity are manifested not only in terms of cellular adhesion but also in traits such as invasion, ECM degradation, and proliferation, which may be modulated in association with or independently of the former. Future iterations of the model will incorporate signaling networks that link multiple traits (such as coupling the EMT network with Notch-Delta signaling that enables 'salt-and-pepper'

Please cite this article in press as: Prasanna et al., Spatial heterogeneity in tumor adhesion qualifies collective cell invasion, Biophysical Journal (2024), https://doi.org/10.1016/j.bpj.2024.05.005

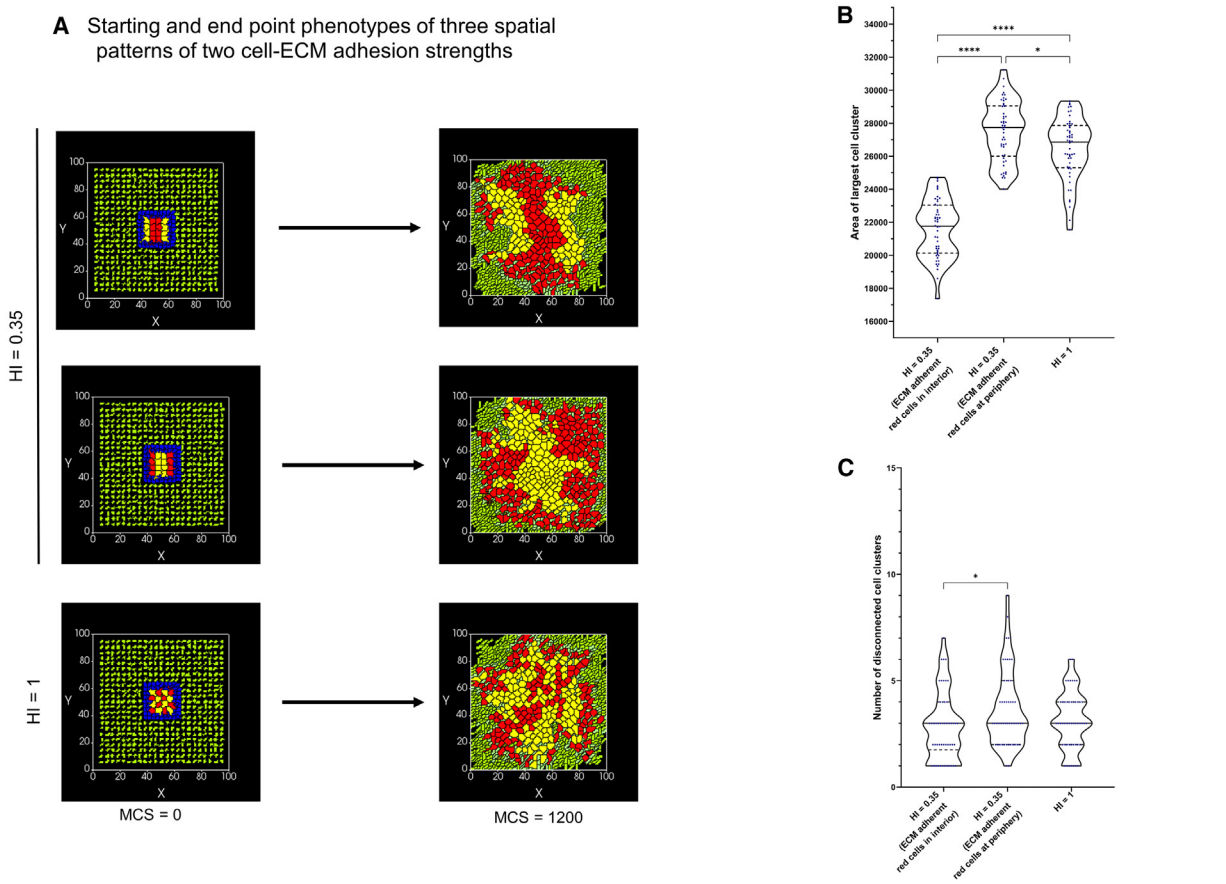

FIGURE 7 Special cases of starting spatial patterns with HI smaller than high HI showing higher and lower invasion for cell-ECM adhesion strength variation. (*A*) Start and endpoint phenotypes of three spatial patterns with cell-ECM adhesion being double of model cell-ECM adhesion for red cells and half for yellow cells. (*B*) Violin plot with median of area of largest cell cluster for spatial patterns with HI = 0.35 (where the red cells are localized inside and outside, respectively) and HI = 1. Statistical significance for the measurements in the simulations was computed using one-way ANOVA with Tukey-Kramer post hoc comparisons. Significance (p value) is represented as *, where *$p \leq 0.05$, **$p \leq 0.01$, ***$p \leq 0.001$, and ****$p < 0.0001$. (*C*) Violin plot with median of number of disconnected cell clusters for spatial patterns with HI = 0.35 and HI = 1. To see this figure in color, go online.

patterns) (47) and which may be amenable to variation in signaling strengths indicative of the consequences of genetic and epigenetic aberrations. Our investigations in this article examine heterogeneity in adhesion within the parametric constraints of CCI. Our next effort will be focused on examining the effects of spatial variation in adhesion under initial conditions of dispersed or multimodal invasions.

We conclude by highlighting the broader implications of our study: although our model is motivated in its assumptions and histopathological foundations by tumorigenic context, the framework itself is as easily adaptable to embryological problems wherein CCI has been found to play a role in several organogenetic systems such as glandular morphogenesis, gastrulation, somitogenesis, and limb development. There is burgeoning evidence through single-cell sequencing for the presence of cellular heterogeneity within developing tissues and organs during embryogenesis: in fact, polyclonal modes of embryogenesis have been reported across diverse phyla (48). Our results suggest that adhesion heterogeneity allows a cellular population to invade effectively while also retaining evolvability toward switching between multicellular to unicellular phenotypes. A translational ramification of our study is that interactions based on differential adhesions can mediate qualitative shifts in the "graininess" of niche heterogeneity in growing tumoroid populations. Cellular masses that start out with finely intermingled niches may show niche-sorting during their progression: biopsying such tumors at a single spatial locus may lead to an underestimation of intratumoral heterogeneity. Our simulations suggest a multi-temporal multi-locus strategy for the assessment of heterogeneity within malignant tumors. Although not addressed in this manuscript, it is pertinent to ask what may lead to the manifestation of the heterogeneous patterns we have worked with in this paper. Whereas low HI patterns are phenomenologically indicative of differentially sorted cells, demonstrated in tissues with altered adhesion molecules, high HI patterns are suggestive of operational mesoscale signaling of juxtracrine or paracrine nature, such as Notch-Delta signaling

Please cite this article in press as: Prasanna et al., Spatial heterogeneity in tumor adhesion qualifies collective cell invasion, Biophysical Journal (2024), https://doi.org/10.1016/j.bpj.2024.05.005

(49). The interplay between the latter and adhesion will be probed in future studies.

DATA AND CODE AVAILABILITY

The code for the manuscript can be accessed at https://github.com/cvsp-res/spatial_hetero.git.

SUPPORTING MATERIAL

Supporting material can be found online at https://doi.org/10.1016/j.bpj.2024.05.005.

AUTHOR CONTRIBUTIONS

R.B. and M.K.J. framed the problem statement. C.V.S.P. carried out the simulations. R.B., M.K.J., and C.V.S.P. analyzed the results of the simulations. R.B., M.K.J., and C.V.S.P. wrote and edited the manuscript.

ACKNOWLEDGMENTS

This work was supported by Wellcome Trust/DBT India Alliance Fellowship/Grant (IA/I/17/2/503312) awarded to R.B. It was also supported by the John Templeton Foundation (no. 62220), the Indo-French Centre for the Promotion of Advanced Research – CEFIPRA grant (69T08-2) and the International Emerging Actions (328003) to R.B., and a Ramanujan Fellowship (SB/S2/RJN-049/2018) awarded by the Science and Engineering Research Board, Government of India to M.K.J. M.K.J. was also supported by Param Hansa Philanthropies. C.V.S.P. acknowledges support from the Ministry of Education, Government of India, and Axis Bank Ph.D. Fellowship for student scholarship. We wish to thank Prof. Shamik Sen and Dr. Asadullah for their critical comments on the work. The opinions expressed in this paper are those of the authors and not those of the John Templeton Foundation.

DECLARATION OF INTERESTS

The authors do not declare any conflicts of interest.

REFERENCES

1. Wu, J.-S., J. Jiang, …, X.-H. Liang. 2021. Plasticity of cancer cell invasion: Patterns and mechanisms. *Transl. Oncol.* 14:100899. https://doi.org/10.1016/j.tranon.2020.100899.
2. Friedl, P., J. Locker, …, J. E. Segall. 2012. Classifying collective cancer cell invasion. *Nat. Cell Biol.* 14:777–783. https://doi.org/10.1038/ncb2548.
3. Pramanik, D., M. K. Jolly, and R. Bhat. 2021. Matrix adhesion and remodeling diversifies modes of cancer invasion across spatial scales. *J. Theor. Biol.* 524:110733. https://doi.org/10.1016/j.jtbi.2021.110733.
4. Mayor, R., and S. Etienne-Manneville. 2016. The front and rear of collective cell migration. *Nat. Rev. Mol. Cell Biol.* 17:97–109. https://doi.org/10.1038/nrm.2015.14.
5. Vilchez Mercedes, S. A., F. Bocci, …, P. K. Wong. 2021. Decoding leader cells in collective cancer invasion. *Nat. Rev. Cancer.* 21:592–604. https://doi.org/10.1038/s41568-021-00376-8.
6. Ilina, O., P. G. Gritsenko, …, P. Friedl. 2020. Cell-cell adhesion and 3D matrix confinement determine jamming transitions in breast cancer invasion. *Nat. Cell Biol.* 22:1103–1115. https://doi.org/10.1038/s41556-020-0552-6.
7. Pally, D., S. Goutham, and R. Bhat. 2022. Extracellular matrix as a driver for intratumoral heterogeneity. *Phys. Biol.* 19. https://doi.org/10.1088/1478-3975/ac6eb0.
8. Alexander, J., O. Mariani, …, R. Natrajan. 2022. Assessment of the Molecular Heterogeneity of E-Cadherin Expression in Invasive Lobular Breast Cancer. *Cancers.* 14:295. https://doi.org/10.3390/cancers14020295.
9. Berx, G., and F. Van Roy. 2001. The E-cadherin/catenin complex: an important gatekeeper in breast cancer tumorigenesis and malignant progression. *Breast Cancer Res.* 3:289–293. https://doi.org/10.1186/bcr309.
10. Harryman, W. L., K. D. Marr, …, A. E. Cress. 2022. Integrins and Epithelial-Mesenchymal Cooperation in the Tumor Microenvironment of Muscle-Invasive Lethal Cancers. *Front. Cell Dev. Biol.* 10:837585. https://doi.org/10.3389/fcell.2022.837585.
11. Bierie, B., S. E. Pierce, …, R. A. Weinberg. 2017. Integrin-β4 identifies cancer stem cell-enriched populations of partially mesenchymal carcinoma cells. *Proc. Natl. Acad. Sci. USA.* 114:E2337–E2346. https://doi.org/10.1073/pnas.1618298114.
12. Wu, H.-J., D. Temko, …, F. Michor. 2022. Spatial intra-tumor heterogeneity is associated with survival of lung adenocarcinoma patients. *Cell Genom.* 2:100165. https://doi.org/10.1016/j.xgen.2022.100165.
13. Fuhs, T., F. Wetzel, …, J. A. Käs. 2022. Rigid tumours contain soft cancer cells. *Nat. Phys.* 18:1510–1519. https://doi.org/10.1038/s41567-022-01755-0.
14. Han, Y. L., A. F. Pegoraro, …, M. Guo. 2020. Cell swelling, softening and invasion in a three-dimensional breast cancer model. *Nat. Phys.* 16:101–108. https://doi.org/10.1038/s41567-019-0680-8.
15. Pally, D., D. Pramanik, …, R. Bhat. 2021. Heterogeneity in 2,6-Linked Sialic Acids Potentiates Invasion of Breast Cancer Epithelia. *ACS Cent. Sci.* 7:110–125. https://doi.org/10.1021/acscentsci.0c00601.
16. Asadullah, S. K., N. Saxena, …, S. Sen. 2021. Combined heterogeneity in cell size and deformability promotes cancer invasiveness. *J. Cell Sci.* 134:jcs250225. https://doi.org/10.1242/jcs.250225.
17. Hallou, A., J. Jennings, and A. J. Kabla. 2017. Tumour heterogeneity promotes collective invasion and cancer metastatic dissemination. *R. Soc. Open Sci.* 4:161007. https://doi.org/10.1098/rsos.161007.
18. Bhaskar, D., W. Y. Zhang, …, I. Y. Wong. 2023. Topological data analysis of spatial patterning in heterogeneous cell populations: clustering and sorting with varying cell-cell adhesion. *NPJ Syst. Biol. Appl.* 9:43. https://doi.org/10.1038/s41540-023-00302-8.
19. Maître, J.-L., H. Berthoumieux, …, C. P. Heisenberg. 2012. Adhesion Functions in Cell Sorting by Mechanically Coupling the Cortices of Adhering Cells. *Science.* 338:253–256. https://doi.org/10.1126/science.1225399.
20. Malmi-Kakkada, A. N., S. Sinha, …, D. Thirumalai. 2022. Adhesion strength between cells regulate nonmonotonic growth by a biomechanical feedback mechanism. *Biophys. J.* 121:3719–3729. https://doi.org/10.1016/j.bpj.2022.04.032.
21. Amack, J. D., and M. L. Manning. 2012. Knowing the Boundaries: Extending the Differential Adhesion Hypothesis in Embryonic Cell Sorting. *Science.* 338:212–215. https://doi.org/10.1126/science.1223953.
22. Reher, D., B. Klink, …, A. Voss-Böhme. 2017. Cell adhesion heterogeneity reinforces tumour cell dissemination: novel insights from a mathematical model. *Biol. Direct.* 12:18. https://doi.org/10.1186/s13062-017-0188-z.
23. Okegawa, T., Y. Li, …, J.-T. Hsieh. 2002. Cell adhesion proteins as tumor suppressors. *J. Urol.* 167:1836–1843.
24. Pajic-Lijakovic, I., M. Milivojevic, and A. G. Clark. 2022. Collective Cell Migration on Collagen-I Networks: The Impact of Matrix Viscoelasticity. *Front. Cell Dev. Biol.* 10:901026. https://doi.org/10.3389/fcell.2022.901026.
25. Ravasio, A., A. P. Le, …, B. Ladoux. 2015. Regulation of epithelial cell organization by tuning cell-substrate adhesion. *Integr. Biol.* 7:1228–1241. https://doi.org/10.1039/c5ib00196j.

26. Leggett, S. E., A. M. Hruska, …, I. Y. Wong. 2021. The epithelial-mesenchymal transition and the cytoskeleton in bioengineered systems. *Cell Commun. Signal.* 19:32. https://doi.org/10.1186/s12964-021-00713-2.

27. Lamouille, S., J. Xu, and R. Derynck. 2014. Molecular mechanisms of epithelial-mesenchymal transition. *Nat. Rev. Mol. Cell Biol.* 15:178–196. https://doi.org/10.1038/nrm3758.

28. Yang, Y., H. Zheng, …, S. Fan. 2019. An emerging tumor invasion mechanism about the collective cell migration. *Am. J. Transl. Res.* 11:5301–5312.

29. Tripathi, S., P. Chakraborty, …, M. K. Jolly. 2020. A mechanism for epithelial-mesenchymal heterogeneity in a population of cancer cells. *PLoS Comput. Biol.* 16:e1007619. https://doi.org/10.1371/journal.pcbi.1007619.

30. Kim, J. E., E. Leung, …, G. J. Finlay. 2013. Heterogeneity of expression of epithelial-mesenchymal transition markers in melanocytes and melanoma cell lines. *Front. Genet.* 4:97. https://doi.org/10.3389/fgene.2013.00097.

31. Hong, D., A. J. Fritz, …, G. S. Stein. 2018. Epithelial-to-mesenchymal transition and cancer stem cells contribute to breast cancer heterogeneity. *J. Cell. Physiol.* 233:9136–9144. https://doi.org/10.1002/jcp.26847.

32. Jamal-Hanjani, M., G. A. Wilson; …, TRACERx Consortium. 2017. Tracking the Evolution of Non–Small-Cell Lung Cancer. *N. Engl. J. Med.* 376:2109–2121. https://doi.org/10.1056/NEJMoa1616288.

33. Grosser, S., J. Lippoldt, …, J. A. Käs. 2021. Cell and Nucleus Shape as an Indicator of Tissue Fluidity in Carcinoma. *Phys. Rev. X.* 11:011033. https://doi.org/10.1103/PhysRevX.11.011033.

34. Andor, N., T. A. Graham, …, C. C. Maley. 2016. Pan-cancer analysis of the extent and consequences of intratumor heterogeneity. *Nat. Med.* 22:105–113. https://doi.org/10.1038/nm.3984.

35. Liu, S., Y. Cong, …, M. S. Wicha. 2014. Breast cancer stem cells transition between epithelial and mesenchymal states reflective of their normal counterparts. *Stem Cell Rep.* 2:78–91. https://doi.org/10.1016/j.stemcr.2013.11.009.

36. Brabletz, T., A. Jung, …, T. Kirchner. 2001. Variable beta-catenin expression in colorectal cancers indicates tumor progression driven by the tumor environment. *Proc. Natl. Acad. Sci. USA.* 98:10356–10361. https://doi.org/10.1073/pnas.171610498.

37. Ghosh, D., J. Hsu, …, M. R. Dawson. 2023. Spatial Heterogeneity in Cytoskeletal Mechanics Response to TGF-β1 and Hypoxia Mediates Partial Epithelial-to-Meshenchymal Transition in Epithelial Ovarian Cancer Cells. *Cancers.* 15:3186. https://doi.org/10.3390/cancers15123186.

38. Bocci, F., L. Gearhart-Serna, …, M. K. Jolly. 2019. Toward understanding cancer stem cell heterogeneity in the tumor microenvironment. *Proc. Natl. Acad. Sci. USA.* 116:148–157. https://doi.org/10.1073/pnas.1815345116.

39. Vilchez Mercedes, S. A., F. Bocci, …, P. K. Wong. 2022. Nrf2 Modulates the Hybrid Epithelial/Mesenchymal Phenotype and Notch Signaling During Collective Cancer Migration. *Front. Mol. Biosci.* 9:807324. https://doi.org/10.3389/fmolb.2022.807324.

40. Zhang, J., K. F. Goliwas, …, C. A. Reinhart-King. 2019. Energetic regulation of coordinated leader-follower dynamics during collective invasion of breast cancer cells. *Proc. Natl. Acad. Sci. USA.* 116:7867–7872. https://doi.org/10.1073/pnas.1809964116.

41. de Bruin, E. C., N. McGranahan, …, C. Swanton. 2014. Spatial and temporal diversity in genomic instability processes defines lung cancer evolution. *Science.* 346:251–256. https://doi.org/10.1126/science.1253462.

42. Morris, L. G. T., N. Riaz, …, T. A. Chan. 2016. Pan-cancer analysis of intratumor heterogeneity as a prognostic determinant of survival. *Oncotarget.* 7:10051–10063. https://doi.org/10.18632/oncotarget.7067.

43. Collins, C., A. K. Denisin, …, W. J. Nelson. 2017. Changes in E-cadherin rigidity sensing regulate cell adhesion. *Proc. Natl. Acad. Sci. USA.* 114:E5835–E5844. https://doi.org/10.1073/pnas.1618676114.

44. Borghi, N., M. Sorokina, …, A. R. Dunn. 2012. E-cadherin is under constitutive actomyosin-generated tension that is increased at cell-cell contacts upon externally applied stretch. *Proc. Natl. Acad. Sci. USA.* 109:12568–12573. https://doi.org/10.1073/pnas.1204390109.

45. Hui, T. H., Y. H. Tang, …, Y. Lin. 2018. Cadherin- and Rigidity-Dependent Growth of Lung Cancer Cells in a Partially Confined Microenvironment. *ACS Biomater. Sci. Eng.* 4:446–455. https://doi.org/10.1021/acsbiomaterials.7b00130.

46. Canel, M., A. Serrels, …, V. G. Brunton. 2013. E-cadherin–integrin crosstalk in cancer invasion and metastasis. *J. Cell Sci.* 126:393–401. https://doi.org/10.1242/jcs.100115.

47. Boareto, M., M. K. Jolly, …, J. N. Onuchic. 2016. Notch-Jagged signalling can give rise to clusters of cells exhibiting a hybrid epithelial/mesenchymal phenotype. *J. R. Soc. Interface.* 13:20151106. https://doi.org/10.1098/rsif.2015.1106.

48. Hamant, O., R. Bhat, …, S. A. Newman. 2019. Does resource availability help determine the evolutionary route to multicellularity? *Evol. Dev.* 21:115–119. https://doi.org/10.1111/ede.12287.

49. Jolly, M. K., M. Boareto, …, E. Ben-Jacob. 2015. Operating principles of Notch–Delta–Jagged module of cell–cell communication. *New J. Phys.* 17:055021. https://doi.org/10.1088/1367-2630/17/5/055021.

50. Balter, A., R. M. H. Merks, …, J. A. Glazier. 2007. The Glazier-Graner-Hogeweg Model: Extensions, Future Directions, and Opportunities for Further Study. *In* Single-Cell-Based Models in Biology and Medicine. Birkhäuser Basel, Basel, pp. 151–167. https://doi.org/10.1007/978-3-7643-8123-3_7.

51. Swat, M. H., G. L. Thomas, …, J. A. Glazier. 2012. Multi-scale modeling of tissues using CompuCell3D. *Methods Cell Biol.* 110:325–366. https://doi.org/10.1016/B978-0-12-388403-9.00013-8.